Large-scale molecular dynamics simulations of Kármán vortex and sound wave: cavitation and polymer effects

Yuta Asano [1], Hiroshi Watanabe [2], and Hiroshi Noguchi [1]

[1] *Institute for Solid State Physics,*

The University of Tokyo, Kashiwa-no-ha, Kashiwa, Chiba 277-8581, Japan

[2] *Department of Applied Physics and Physico-Informatics,*

Keio University, Yokohama, Kanagawa 223-8522, Japan

Abstract

In many industrial flows, microscale effects have a significant impact on their macroscale flows. Turbulent drag reduction by polymer addition and cavitation around rotating turbines in water are typical examples. In these flows, phenomena in a wide range of scales coexist, from molecular scale motion to macroscale fluid motion, and these interact with each other under strongly non-equilibrium. Therefore, it is challenging to clarify the underlying mechanism by its complexity.

We have performed large-scale molecular dynamics (MD) simulations of complex flows, such as polymer solutions and cavitating flow, as well as MD of sound propagation, using the ISSP supercomputer. In this activity report, we present a brief overview of these studies [1-4].

1. Introduction

Fluid flows play a vital role in a wide range of fields, from tap water familiar to our daily lives to fuel pipelines in energy supply systems. It is no exaggeration to say that flow sustains our lives. Therefore, a thorough understanding of the flow phenomena will improve our lives, also significantly contributes to global environmental protection. Flow control in industrial processes is an essential topic in fluid engineering, such as turbulence drag reduction by polymer addition [5] and gas-liquid multi-phase flow due to the cavitation [6]. Thus, many researchers have conducted experiments and numerical simulations based on the Navier—Stokes equation to clarify the mechanisms. However, since various phenomena in a wide range of scales coexist and interact with each other in non-equilibrium, the analyses are challenging issues. Therefore, it is crucial to analyze all phenomena simultaneously, from molecular-scale dynamics to fluid motion to understand the complex flows.

Mesoscale analysis methods such as the lattice Boltzmann method [7] and Multi-particle collision dynamics [8,9] have been developed to analyze the flow considering the effects of molecular-scale dynamics. Also, the micro-

macro coupling approaches [10,11] have been proposed to investigate more detailed molecular-scale information. However, in light of today's computational power, it is possible to simulate flows by all-particle simulations, namely a molecular dynamics (MD) simulation. In the MD simulation, molecular-scale dynamics, such as phase transition and polymer motion, naturally appear in the flow by simply solving the Newtonian equations of motion, only providing the interparticle interactions. In conventional fluid analysis methods, phenomenological models, such as constitutive equations and an equation of state, are required to describe these phenomena. Instead, we have to prepare a sufficiently large computational cell that can resolve the macroscale flow characteristics. Therefore, although it is inevitably a large-scale simulation, it will help us understand complex flow phenomena.

In this report, we present a brief overview of flow analysis by using large-scale MD simulations. We explain the effect of polymer addition and cavitation on the flow around a cylinder in sections 2 and 3, respectively. In section 4, we describe the application to soundwave propagation in a simple fluid. In section 5, we explain the recent study of cavitating flow in a polymer solution. Section 6 is a summary.

2. Effects of polymer addition on Kármán Vortex [1]

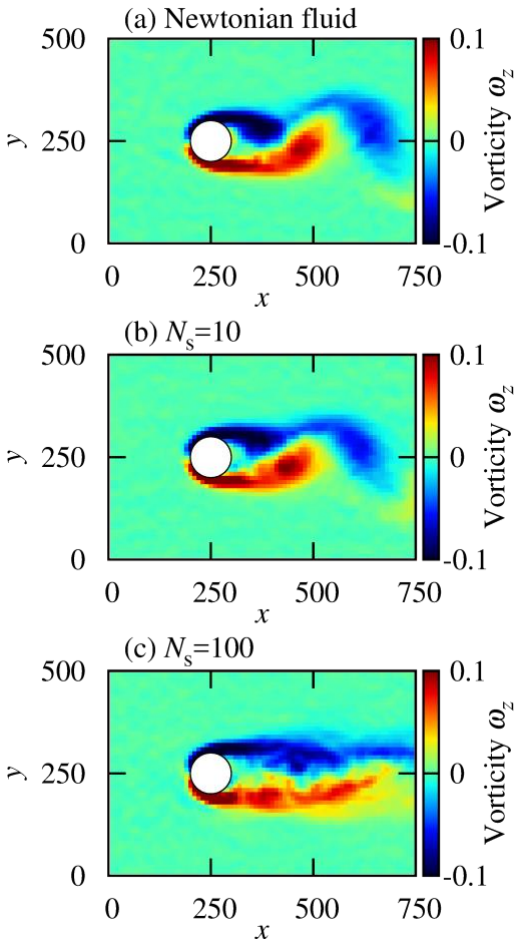

Fig. 1: Instantaneous vorticity fields for (a) the Newtonian fluid, (b) polymer solution with the number of segments $N_s = 10$, and (c) polymer solution with $N_s = 100$ at the Reynolds number $Re = 64$ [1].

Adding a tiny amount of polymer into a Newtonian fluid involves significant changes in the flow characteristics, such as a dramatic reduction in frictional drag [5] and suppression of the Kármán vortex [12]. Since most industrial flows are turbulent, the flow control by adding polymers is an attractive method in engineering applications because it saves energy

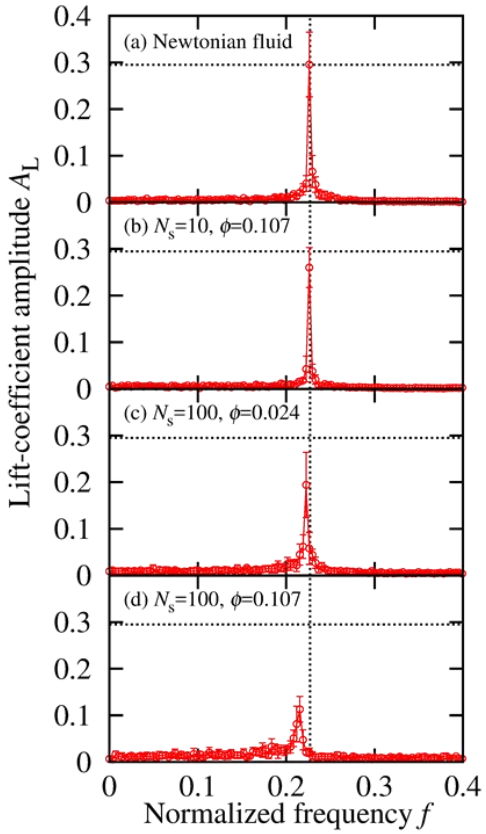

Fig. 2: Fourier spectra of the lift coefficient at $Re = 64$ [1]. (a) Newtonian fluid. (b) Polymer solution with $N_s = 10$ and volume fraction $\phi = 10$. (c) Polymer solution with $N_s = 100$ and $\phi = 0.02$.(d) Polymer solution with $N_s = 100$ and $\phi = 0.107$. The vertical and horizontal dotted lines denote the peak position and height for the Newtonian fluid, respectively.

consumption. However, the mechanism is not well understood because the polymer rheology in a flow is unclear.

The interaction between polymers and vortices presumably plays a significant role in the changes in flow characteristics. Therefore, it is necessary to elucidate the effects of polymers on vortices from the molecular scale. We focus on the flow around a cylinder, which is the most typical flow accompanied by vortices and is suitable for analysis due to its periodicity. We investigate the effects of polymers on vortices in the two-dimensional flow around a circular cylinder by MD simulations.

Figure 1 shows typical snapshots of the vorticity field. As for the Newtonian fluid, an alternating vortex street, the Kármán vortex street, appears behind the cylinder. Similar vortices appear for the short-chain polymers. However, for long-chain polymers, the vortices are blurred. Therefore, the chain length of the polymer significantly affects vortex formation.

Figure 2 shows the Fourier spectra of the lift coefficient. For the Newtonian fluid, a sharp peak appears, which indicates periodic vortex shedding. Note that the peak frequency is slightly increased by the finite size effects we reported in Ref. 13. The short-polymer solution shows a similar sharp peak. On the other hand, the peak position shifts to a lower frequency, and the spectrum broadens for the long-polymer solution. These effects enhance with increasing polymer concentration. The effects of polymer addition on the flow, (1) vortex blurring, (2) frequency reduction, and (3) chain length effect, obtained by MD simulations, are in good agreement with experimental results [12].

Figures 3(a) and 3(b) show the gyration radius of short- and long-chain polymers,

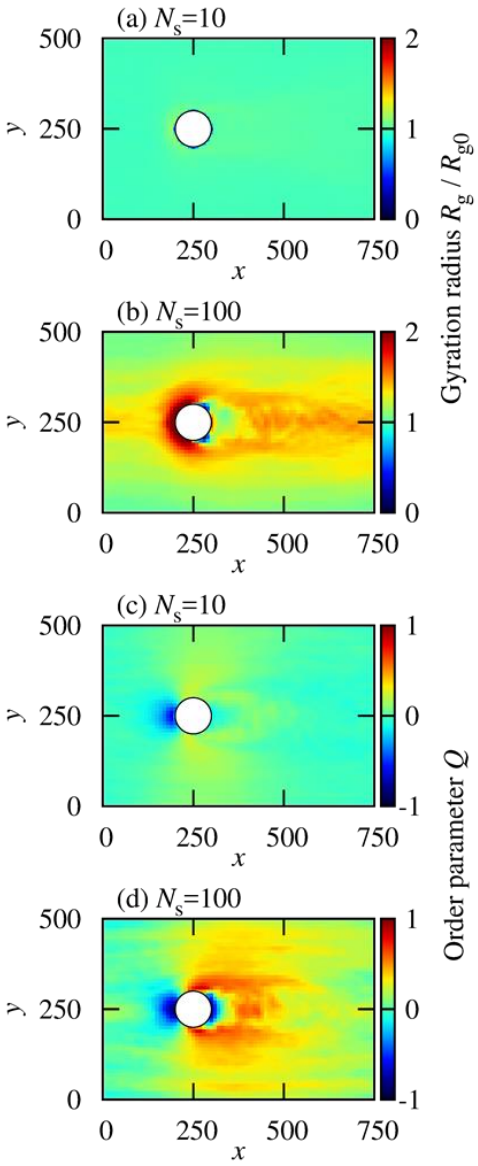

Fig. 3 Spatial distributions of the gyration radius R_g and orientational order Q for the polymer solutions with (a, c) $N_s = 10$ and (b, d) $N_s = 100$ at $Re = 64$ and $\phi = 0.107$[1]. R_{g0} is the gyration radius in the absence of the flow.

respectively. For short-chain polymer, the gyration radius is virtually identical to that in the stationary fluid. Therefore, the polymer flows with an almost spherical shape as a particle. On the other hand, long-chain polymers are significantly stretched near the cylinder and in the vortex behind the cylinder. Furthermore, the vortex also entrains the polymer in its vicinity.

Figures 3(c) and 3(d) show the orientational order Q of the short- and long-chain polymers, respectively. When the polymer aligns in the flow direction, $Q = 1$; the polymer aligns perpendicular to the flow, $Q = -1$; the polymer directs randomly, $Q = 0$. For the short-chain polymer, polymers orient randomly in the entire area. However, for long-chain polymers, the polymers are aligned in the flow direction near the cylinder. Furthermore, the polymers also tend to align in the flow direction in the vortices behind the cylinder. The reduction of the orientational order behind the cylinder is due to the entrainment by the vortex. Therefore, the stretching and entrainment of the polymer play a significant role in vortex suppression. As a consequence, the shapes of the vortices become blurred.

3. Effects of cavitation on the Kármán vortex behind circular-cylinder arrays [2]

Cavitation is a phenomenon of forming bubbles due to local pressure drop in a flowing liquid with high velocity [14]. When cavitation occurs in fluid machinery, such as pumps and turbines, it causes various adverse effects such as performance degradation, noise and vibration, and erosion. Therefore, it is vital in fluid

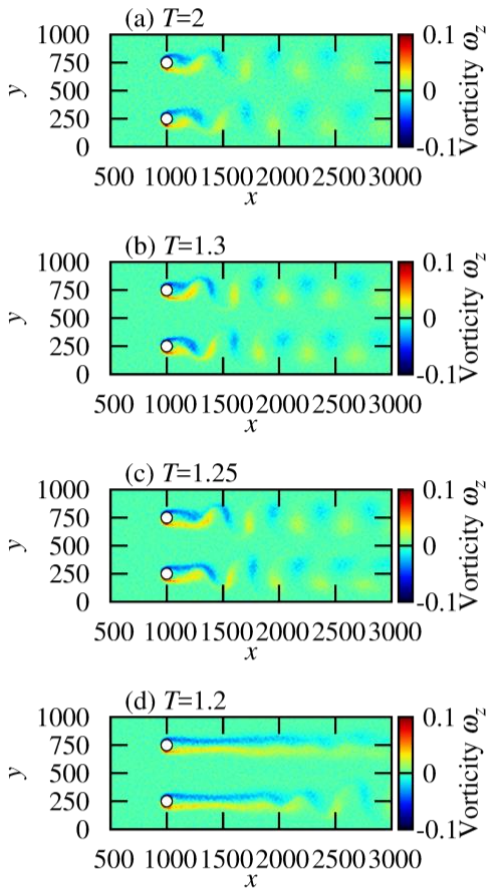

Fig 4: Instantaneous vorticity fields for the (a) non-cavitating flow ($T = 2$) and (b-d) cavitating flows ($T = 1.5$, 1.25, and 1.2) [2].

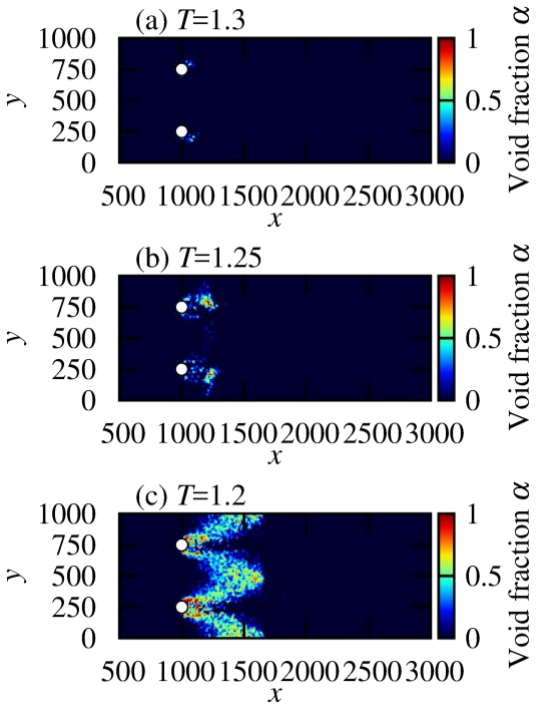

Fig. 5: Instantaneous void fraction fields for (a) $T = 1.3$, (b) $T = 1.25$, and (c) $T = 1.2$ [2].

engineering to clarify the cavitation mechanism for appropriate control of the cavitating flow. However, because of the limitations of discussing the dynamics of microscopic bubble nuclei in a macroscopic flow, the cavitation mechanism is still not understood well. To clarify the effects of cavitation on the flow, we performed a large-scale MD simulation of the flow for the Lennard-Jones (LJ) around cylinders in a side-by-side arrangement.

Figures 4 and 5 show the typical snapshots of the vorticity and void fraction field, respectively. At high temperature ($T = 2$), no bubbles appear (i.e., non-cavitating flow). The Kármán vortex appears behind the cylinders, and the upper and lower vortex streets synchronize in anti-phase. As temperature decreases, bubbles appear in the vicinity of the cylinder at $T = 1.3$ in conjunction with vortex shedding (Fig. 5 (a)). The vortex streets behind the cylinder synchronize in anti-phase, as in the case of $T = 2$ (Figs. 4(a) and 4(b)).

At $T = 1.25$, the gas phase region is formed behind the cylinder and is attached to the cylinder (Fig. 5(b)). Also, the phase difference between the upper and lower vortex streets

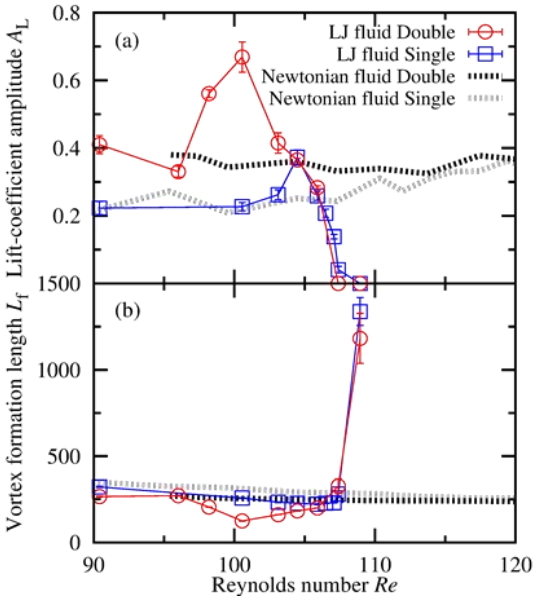

Fig. 6: Re dependence of (a) the lift coefficient amplitude and (b) vortex formation for the LJ fluid and Newtonian fluid [2]. Double and Single in the legend denote two- and one-cylinder systems, respectively.

slightly shifts (Fig. 4(c)). At $T = 1.2$, the gas phase region behind the cylinder expands further (Fig. 5. (c). In addition, the upper and lower vortex structures become asymmetric (Fig. 4(d)). This asymmetric vortex structure switches over a long period. For the fluid without phase transition, such a change in the flow field does not occur with temperature change. We found that the density fluctuation caused by the bubble generation has a significant effect on the vortex structure.

As the vortex structure changes, the lift force acting on the cylinder is also affected. Figure 6(a) shows the Redependence of the amplitude of the lift coefficient A_L and the vortex formation length L_f. For comparison, the figure also shows the results for the Newtonian fluid. For the reference liquid, A_L and L_f tend to increase and decrease with increase Re, respectively. However, in the case of LJ fluids, they exhibit non-monotonic behavior to Re. This behavior is probably due to the conflicting effects of increasing Re and bubble generation. A_L rapidly decreases and finally disappears due to the bubble generation. Simultaneously with the disappearance of A_L, L_f rapidly increases.

For the Newtonian fluid, A_L and L_f show almost the same trend for the two-cylinder system and the one-cylinder system, which has only one cylinder with the same distance between the neighboring (periodic image) cylinders (the vortex streets are always synchronized in-phase). In the case of LJ fluid, however, the behavior before bubble generation is different. The upward and downward peaks appear in A_L and L_f, respectively. Their positions for one- and two-cylinder systems are $Re = 105$ and 101, respectively. These peaks are probably due to a small nucleus generation which is the precursor of the cavitation or density fluctuations originating from the critical phenomena. Since the phase retraction amplifies the oscillation amplitude, the peak appears at a higher temperature in the two-cylinder system than in the one-cylinder system. After bubble generation, the bubbles weaken the interference between the vortex street, and the effect of the

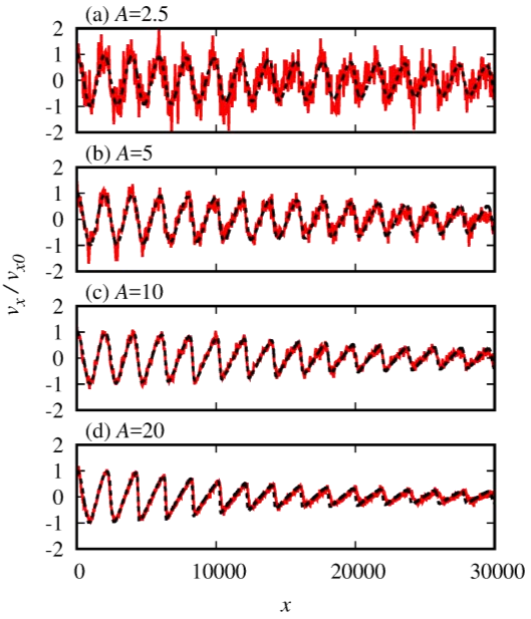

Fig 7: Waveforms of the LJ fluid for the (a) amplitude $A = 2.5$ (b) $A = 5$ (c) $A = 10$, and (d) $A = 20$ at frequency $f = 0.001$ [3]. The red and black lines represent the results of MD simulation and the Burgers' equation, respectively.

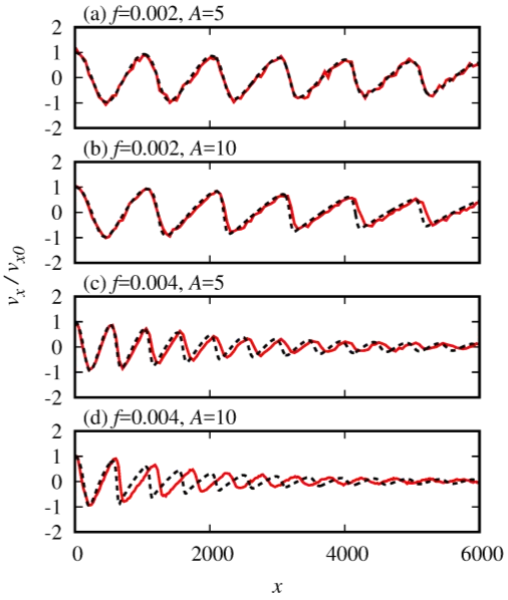

Fig. 8: Waveforms of the LJ fluid for the (a) $f = 0.002$ and $A = 5$, (b) $f = 0.002$ and $A = 10$ (c) $f = 0.004$ and $A = 5$, and (d) $f = 0.004$ and $A = 10$ [3]. The red and black lines represent the results of MD simulation and the Burgers' equation, respectively.

phase difference is almost negligible. We found that the bubble generation significantly affects the vortex structures, vortex interference, and lift due to vortex shedding.

4. Soundwave propagation in simple fluid [3]

Sound waves are a familiar phenomenon in our daily lives, such as the voices and sound of musical instruments. Because of the sound properties of propagating a wide range of solid, liquid, and gaseous materials, their application exists in a wide range of engineering fields. In particular, applications of ultrasonic cavitation extend in a wide range of applications, such as medical treatment and food processing. For these applications, it is crucial to understand the characteristics of ultrasonic cavitation and the propagation in complex fluids. Therefore, it is necessary to analyze the sound wave propagation from the molecular scale.

We apply the MD simulation to the sound propagation in the LJ fluid. Moreover, we perform the fluid dynamics calculation utilizing Burgers' equation to justify the validity of the MD simulation for the sound waves. When the same fluid is analyzed, the two results should

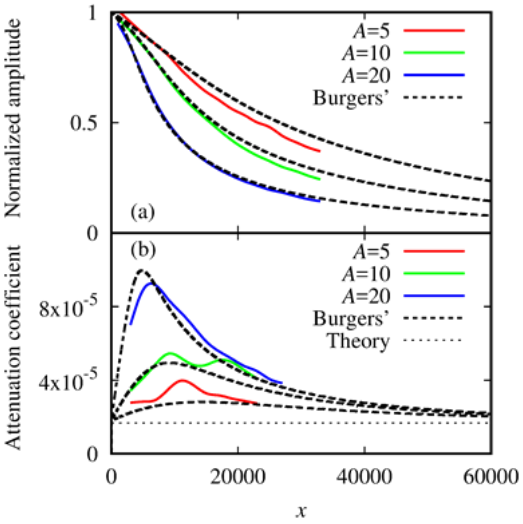

Fig. 9: x dependences of the (a) normalized amplitude and (b) attenuation coefficient of the LJ fluid [3]. The solid and broken lines represent the results of MD simulation and Burgers' equation, respectively. The dotted line in panel (b) shows the classical attenuation coefficient.

agree within the statistical error.

Figure 7 shows the amplitude dependence of the waveform of the LJ fluid at frequency $f = 0.001$. For small amplitudes, the waveform is sinusoidal owing to the weak nonlinearity. As the amplitude increases, the waveform becomes a sawtooth waveform (Figs. 7(c) and 7(d)). The black dotted lines in Fig. 7 are the numerical solutions of Burgers' equation, which is in good agreement with the results of the MD simulation.

Figure 8 shows the frequency dependence of the waveform at higher frequencies. As the frequency increases, the waveforms of the MD simulation and Burgers' equation become deviate; the magnitude of the deviations becomes greater for higher amplitudes. This deviation is due to the acoustic flow that occurs by the high nonlinearity owing to high frequency. Since Burgers' equation is not applicable in the region where acoustic flow occurs, a fluid analysis involving higher-order terms is necessary for a quantitative discussion. The MD simulation provides a waveform reflecting the nonlinearity, thus obtaining a frequency-dependent sound speed.

The attenuation coefficient of a sound wave is estimated from the decrement in amplitude. Figure 9(a) shows the amplitude decrement at $f = 0.001$. When the amplitude is small, the deviation of the MD simulation from the Burgers' equation is slightly different due to the thermal fluctuations. As the amplitude increases, the agreement between them becomes better. We estimate the attenuation coefficient by the logarithmic decrement rate of the amplitude at each position x. Figure 9(b) shows the attenuation coefficient as a function of x. The dotted line shows the value of the attenuation coefficient evaluated from the classical theory. The results of the Burgers' equation approach asymptotically to the classical attenuation coefficient at a sufficient distance from the sound source position ($x = 0$). Although the results of the MD simulation are in good agreement with the results of Burgers' equation when the amplitude is large, the attenuation is overestimated by the nonlinearity. On the other

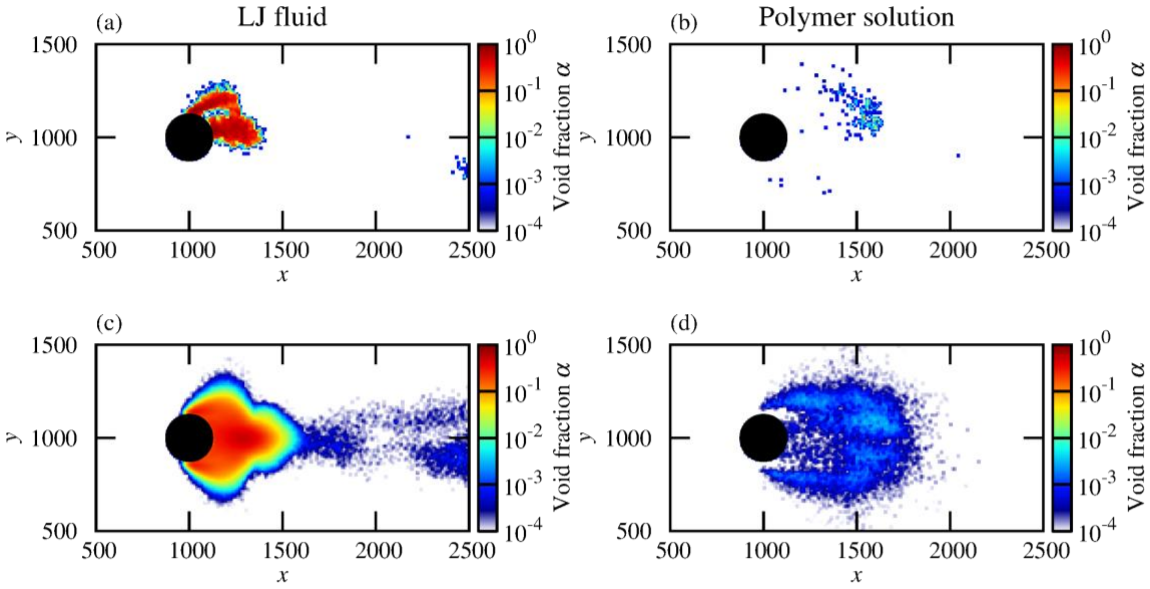

Fig. 10: Instantaneous void fraction fields of the (a) LJ fluid and (b) polymer solution, and time-averaged void fraction of the (c) LJ fluid and (d) polymer solution at $T = 1.25$ [4].

hand, the attenuation coefficient is hardly estimated for small amplitudes due to thermal fluctuation. Therefore, to obtain the classical attenuation coefficient by the MD simulation, the practical method is to estimate the parameters of the Burgers' equation from the waveform of MD simulation.

5. Effects of the polymer addition on the cavitating flow [4]

Finally, we briefly describe our recent analysis on the cavitating flow. In extreme cases, the adverse effects on fluid machinery caused by cavitation are prevented by controlling the flow to suppress cavitation. However, in general, most industrial flows are highly irregular turbulent fields, and it is difficult to achieve such flows by mechanical design. Since polymer addition is one of the methods to realize such flows, it has attracted attention. Although it is challenging to simultaneously analyze polymer motion, bubble nucleus dynamics, and macroscopic flow, the analysis should be possible by integrating the methods described in Sections 2 and 3. Here we briefly describe only the main results.

We investigate the effect of the polymer addition on the cavitating flow around a circular cylinder. Figure 10 shows the distribution of void fraction in the cavitating flow of the LJ fluid at $T = 1.25$, at which the cavitation occurs as described in Sec. 3. The polymer addition dramatically suppresses the formation of bubbles. Note that the polymer addition has negligible effects on the phase transition in the absence of the flow. From the temperature change in the fluid element and the conformation change in the polymer, we found

that the vortex suppression and the entropic elasticity by the polymer have essential roles in the suppression of cavitation.

6. Summary

We performed large-scale MD simulations for complex fluids involving polymers, gas-liquid multi-phase flows owing to cavitation, and sound waves. The direct analysis from the molecular scale enables us to analyze the flow field reflecting the micro-scale effects, such as the elongation properties of polymers, phase transitions that are difficult to model by conventional computational fluid dynamics. In particular, we were able to analyze cavitation in complex fluids, which was one of the main objectives at the beginning of our research. This achievement would not have been possible without using the ISSP supercomputer system B (Ohtaka).

Compared to conventional fluid analysis methods, MD simulation does not require phenomenological models such as equations of state. The advantage of MD simulations is that all physical quantities and phenomena are obtained from molecular motion. Therefore, the MD simulation is a suitable tool to analyze complex flow phenomena, such as the multi-phase and multi-component flow around a propeller.

Acknowledgment

We thank Toshihiro Kawakatsu, Youhei Morii, Shinichi Tsuda, Yuichi Kunishima, and Yuji Higuchi for helpful discussions. This research was supported by MEXT as “Exploratory Challenge on Post-K computer” (Challenge of Basic Science Exploring Extremes through Multi-Physics and Multi-Scale Simulations) and JSPS KAKENHI (Grant No. JP19H05718). We acknowledge the Supercomputer Center, Institute for Solid State Physics (ISSP), University of Tokyo, Research Center for Computational Science (RCCS), Okazaki, Japan, and Center for Computational Materials Science, Institute for Materials Research (IMR), Tohoku University for the use of their supercomputers (Project No.20S0026 for MASAMUNE-IMR in IMR).

References

[1] Y. Asano, H. Watanabe, and H. Noguchi, J. Chem. Phys. **148** (2018) 144901.

[2] Y. Asano, H. Watanabe, and H. Noguchi, J. Chem. Phys. **152** (2020) 034501.

[3] Y. Asano, H. Watanabe, and H. Noguchi, J. Chem. Phys. **153** (2020) 124504.

[4] Y. Asano, H. Watanabe, and H. Noguchi, J. Chem. Phys. **155** (2021) 014905.

[5] G. E. Gadd, Nature **206** (1965) 463.

[6] R. E. Arndt, Ann. Rev. Fluid Mech. **34** (2002) 143.

[7] S. Succi, *The Lattice Boltzmann Equation: For Fluid Dynamics and Beyond*, Oxford University Press Inc., New York (2001).

[8] R. Kapral, Adv. Chem. Phys. **140** (2008) 89.

[9] G. Gompper, T. Ihle, D. M. Kroll, and R. G. Winkler, Adv. Polym. Sci. **221** (2009) 1.

[10] T. Murashima, ISSP Supercomputer Activity Report 2015 (2015) 35.

[11] X. Xu and P. Yu, J. Non-Newtonian Fluid Mech. **229** (2016) 27.

[12] J. R. Cressman, Q. Bailey, and W. I. Goldburg, Phys. Fluids **13** (2001) 867.

[13] Y. Asano, H. Watanabe, and H. Noguchi, J. Phys. Soc. Jpn. **88**, 075003 (2019).

[14] C. E. Brennen, *Cavitation and Bubble Dynamics*, Oxford University Press, (1995).